Inexpensive Methodology to Prepare TiO2 / CuInS2 Hetero-Junctions for Photovoltaic Applications

Inexpensive Methodology to Prepare TiO_2 / $CuInS_2$ Hetero-Junctions for Photovoltaic Applications

Y. Di Iorio and M. Vázquez *

División Electroquímica y Corrosión, INTEMA, CONICET

Facultad de Ingeniería, Universidad Nacional de Mar del Plata

Juan B. Justo 4302 – B7608FDQ Mar del Plata, Argentina

* corresponding author

División Electroquímica Aplicada, INTEMA, UNMdP, CONICET

Juan B. Justo 4302 – B7608FDQ Mar del Plata – Argentina

e-mail: mvazquez@fi.mdp.edu.ar

Tel.: +54 223 481 6600, Fax: +54 223 481 0046

March 21, 2017

Abstract

TiO_2 and $CuInS_2$ (CIS) hetero-junctions were prepared using low-cost, solution-based techniques. Using conducting glass (FTO) as substrate, a thin film of TiO_2 and an ultrathin film of In_2S_3 that acts as buffer layer were deposited by spray pyrolysis. CIS was electrodeposited on top of this duplex layer, at pH 8, room temperature and at constant potential.

A solar cell consisting of FTO/TiO_2/In_2S_3/CIS/graphite was built in superstrate configuration. Morphology, thickness, crystalline structure and chemical composition were analyzed by electronic microscopy, X-Ray diffraction and Raman spectroscopy. $CuInS_2$ films were found to be crystalline with a thickness of 0.4 μm and showed good adhesion. Current-voltage curves in the dark and under illumination proved that the solution-based and vacuum-free deposition of these materials has promising photovoltaic applications. Different thicknesses of the buffer layer were evaluated and the best results were found for In_2S_3 layers deposited with 6 spray cycles. The best solar cell performance showed an efficiency equal to 3.3 % with a V_{oc}= 0.583 V, J_{sc}= 17.7 mA/cm^2, FF = 0.32.

Keywords:

Sulfides ; Growth from solutions ; Hetero-junction semiconductor devices ; Semiconducting indium compounds

1. INTRODUCTION

It is well-known that various types of chalcopyrites, namely $CuInS_2$ (CIS), $CuInSe_2$ (CISe) and $Cu(In,Ga)Se_2$ (CIGS) are frequently used as absorbers for solar cells due to their excellent optical properties [1]. In particular, CIS has several interesting characteristics including high absorption coefficient (around of 10^5 cm^{-1}) at $\lambda \sim 500$ nm [2] and direct band gap optical (E_g) value within 1.3–1.5 eV [3-5], which is close to the optimum range for photovoltaic conversion. $CuInS_2$ is also highly regarded for being environmentally friendly, principally when compared to $CuInSe_2$ where the high toxicity of Se represents a disadvantage during preparation and disposal of the cells. With $CuInS_2$ as absorbing material in a solar cell, typical conversion efficiencies of around 5% have been achieved using atomic layer deposition (ALD) [6-8] and spray pyrolysis deposition [9-13].

At the same time, anatase TiO_2 has an indirect band gap of 3.25 eV [14] and its conduction band is located 4.7 eV below vacuum level, and below the conduction band of CIS. It also has good adherence to glass and can be used as substrate for CIS films deposition.

Solar cells that combine CIS and TiO_2 are not uncommon, most of them being dye-sensitized and quantum dot solar cells [15-19]. Superstrate cells usually show lower efficiencies but are, nevertheless, being actively investigated, particularly when they are processed by non-vacuum methods. Dehghani [20] and Cheshme Khavar [9, 21, 22] have recently published results for totally solution solar cells in superstrate configuration (FTO/TiO_2/In_2S_3/CIS/carbon). Conversion efficiencies approach 3% with CIS inks prepared using a hot injection process [9], up to 5.2% for CIS inks deposited by spin coating [20, 22] and 2.67% when all the layers are deposited by spin coating of molecular

precursor inks [21]. A solar cell combining CIS and TiO_2 deposited by spray pyrolysis has been reported before by O'Hayre et al. [11]. These cells also included a nanostructured TiO_2 layer deposited by doctor blade. The best performance (3.0% efficiency) was achieved from a device with TiO_2 matrix thickness ≈ 200 nm, In_2S_3 buffer layer thickness ≈ 60 nm, and TiO_2 nanoparticulate size = 300 nm. Another successful report of cells with similar materials, deposited by spray pyrolysis has been published by Nguyen et al. [23], but in this case Na doping was necessary to enhance the efficiency. The best efficiency of 2.88 % was obtained at the Na-doping concentration of 4 %.

As for most chalcopyrite solar cells, a buffer layer is typically required between the n-type and p-type regions to improve band alignment[9, 11, 23-25] and other interfacial properties.

The aim of this work is to prepare np junctions with an acceptable photovoltaic response and using exclusively cost-effective deposition methods. A dense TiO_2 film, followed by a thin In_2S_3 buffer layer, was deposited by spray pyrolysis. On top of this bi-layer a $CuInS_2$ film was electrodeposited at room temperature and pH 8. The resulting Cd-free superstrate solar cell, produced at low temperature and with no vacuum-step, no Na doping and no nanostructured layer has not been reported before, and generates a high-current density, comparable to that of vacuum-based CIS solar cells.

2. METHODS

2.1 Substrate

Glass coated with a fluorine doped tin oxide (FTO, SnO_2:F, Libbey Owens Ford, TEC 8/3: resistivity 8 Ω/sq, glass thickness 3 mm) was used as substrate. The glass was

pretreated as described elsewhere[3, 26, 27] and cut into square pieces (2 x 2 cm^2). The active geometrical area was limited to 1.22 cm^2 by the electrochemical cell design.

2.2 Deposition of TiO_2 thin films

FTO squares (2 x 2 cm^2) were placed in a hot plate at 350 ºC and were coated with a compact TiO_2 layer using manual spray pyrolysis deposition with an "in-house" design set-up. A precursor solution containing 2.7 mL titanium (IV) isopropoxide (TTIP) as a titanium source, 3.6 mL acetylacetone (AcAc) as a stabilizer and 54 mL ethanol as solvent was prepared. The solution was atomized by a pneumatic spray (with oxygen as gas carrier) in a 10-cycles process with 30 s of spraying followed by a 1 min delay. More details of the set-up and a full characterization of this layer are given elsewhere [25, 26, 28]. After the spraying process, the samples were kept in the hot plate for 30 minutes at 450 ºC to enhance the crystalline degree of the TiO_2 film. The samples were then allowed to cool down to room temperature.

2.3 Deposition of In_2S_3

An ultrathin layer of In_2S_3 was deposited by spray pyrolysis at 300 ºC on top of the TiO_2 film prior to the deposition of the $CuInS_2$. It is intended to act as buffer layer and minimize any potential mismatch between the valence bands of the n and p semiconductors [10, 11]. The deposition conditions followed those reported earlier by other authors [11, 29]. An aqueous solution containing 0.12 mol L^{-1} of thiourea and 0.018 mol L^{-1} of $InCl_3$ was atomized using N_2 as a carrier gas, in pulses of 30 seconds with 1 minute of delay. 3, 6, 9, 12 and 15 cycles were tested. The best results were obtained

spraying a volume of 25 mL over 6 cycles (less than 100 nm) and these are the results that will be presented below. This value is in agreement with that from O'Hayre et al., who worked with the same combination of materials and determined an optimum thickness of 60 nm for the buffer layer [11]. After the spraying process, the samples were kept on the hot plate at the spraying temperature for 30 minutes to enhance the crystallization process.

2.4 CIS electrochemical deposition

$CuInS_2$ was electrodeposited on top of FTO/TiO_2/In_2S_3 substrates following the procedure described in our previous work [3]. Briefly, the electrodeposition of the CIS films was carried out using a standard three-electrode cell; a saturated calomel electrode (SCE) and a Pt mesh of big area were used as reference and counter electrodes respectively. A constant potential (E = -1.2 V vs SCE) was applied using a Voltalab PGP 201 potentiostat and a stagnant solution at 30ºC.

The electrolytic bath consisted of an aqueous solution containing 0.01 mol L^{-1} $CuCl_2$ (Sigma-Aldrich, purity > 97%), 0.01 mol L^{-1} $InCl_3$ (Sigma-Aldrich, purity > 97%), 0.50 mol L^{-1} Na_2SO_3 (Cicarelli, purity > 99%) and 0.2 mol L^{-1} $Na_3C_3H_5O(COO)_3$ (Biopack, purity > 99%). Sodium citrate (CitNa) was introduced as complexing agent. The solution was stirred continuously during 1 hour. The pH value of the electrolytic bath was adjusted to 8 by the addition of HCl or NaOH from stock solutions. The deposits were rinsed with distilled water and dried in air. Then, an annealing step was undertaken in sulfur vapor atmosphere (sulfur powder at 450º C) for 90 minutes using a purpose-built reactor consisting of a quartz tube furnace [25]. After the thermal treatment, unreacted secondary phases were chemically etched by immersion in 0.5 mol L^{-1} KCN

solutions during 30 s [30]. During the etching process, Cu(I) and Cu(II) sulfides dissolve, forming Cu cyanides and Cu cyanocuprates.

2.5 Characterization

X-ray diffractograms were recorded at grazing incidence (GXRD) using a PANalytical X'Pert Pro diffractometer, Cu-Kα (λ=1.541 Å) radiation at 40 kV and 40 mA. A scan was performed at 0.02 º/s, between 20º and 70º. X´Pert HighScore software was used to analyze the results.

An Invia Reflex confocal Raman microprobe was employed to register localized Raman spectra, in backscattering configuration using a 50x objective and a 785 nm laser.

Images of the layers were recorded with scanning electron microscopy (SEM), using a JEOL JSM-6460LV microscope.

The thickness of each layer was measured using a KLA TENCOR D-100 profilometer.

To evaluate the optical properties of the films, spectra were registered using an UV/Vis/NIR spectrophotometer (Shimadzu 3600 plus) in the wavelength range 350-1100 nm at room temperature.

Current–voltage curves were recorded in the dark and under simulated solar irradiation. Details of the experimental set-up were given before [26, 27]. Alfa-Aesar graphite ink was used to paint dots that were used as back contacts. The electroactive area was 0.01 cm^2. A 150 W Xe lamp with a 380 nm UV-filter attached was used as light source. The light intensity was determined using a Si photodiode, the power of the simulated light was calibrated to AM 1.5 (100 mW cm^{-2}). An IVIUM® compact potentiostat was employed to carry out the current-voltage measurements.

3. RESULTS AND DISCUSSION

This work combines previous experience in solar cells using the same substrate, electron collector and buffer layer (FTO/TiO_2/In_2S_3) [31] with the optimum condition for CIS electrodeposition [3]. The effect of various different thicknesses of the buffer layer was explored and the best results (in terms of solar cell efficiency) were found for In_2S_3 layers deposited with 6 spray cycles, so these are the results that are described in detail below.

Figure 1 presents a GXRD diffractogram of the junction composed by FTO/TiO_2/In_2S_3/CIS. The peaks are sharp and their relative intensities agree with those in the TiO_2 diffraction cards (PDF 21-1272) and $CuInS_2$ (PDF 27-0159). The pattern displays an intense peak at 25.28º that corresponds to the (101) plane of TiO_2, indicating that this semiconductor is present in the cell, i.e. it has not dissolved or detached during the depositions of the buffer and the absorbing layers. The characteristic peaks of chalcopyrite structure are also present in the diffractogram such as 27.81º, 46.21º and 55.01º, as expected for the (112), (204) or (220), and (116) or (312) reflections of the $CuInS_2$ phase, respectively. However, peaks corresponding to the In_2S_3 layer cannot be identified, probably because the thickness of this layer is too thin. Also, the main peak is masked by the FTO signal. No additional phase formation could be detected using the GXRD results. The diffractogram also shows some unlabeled peaks that correspond to k_β radiation from the X-rays that cannot be filtered due to the low incidence angle.

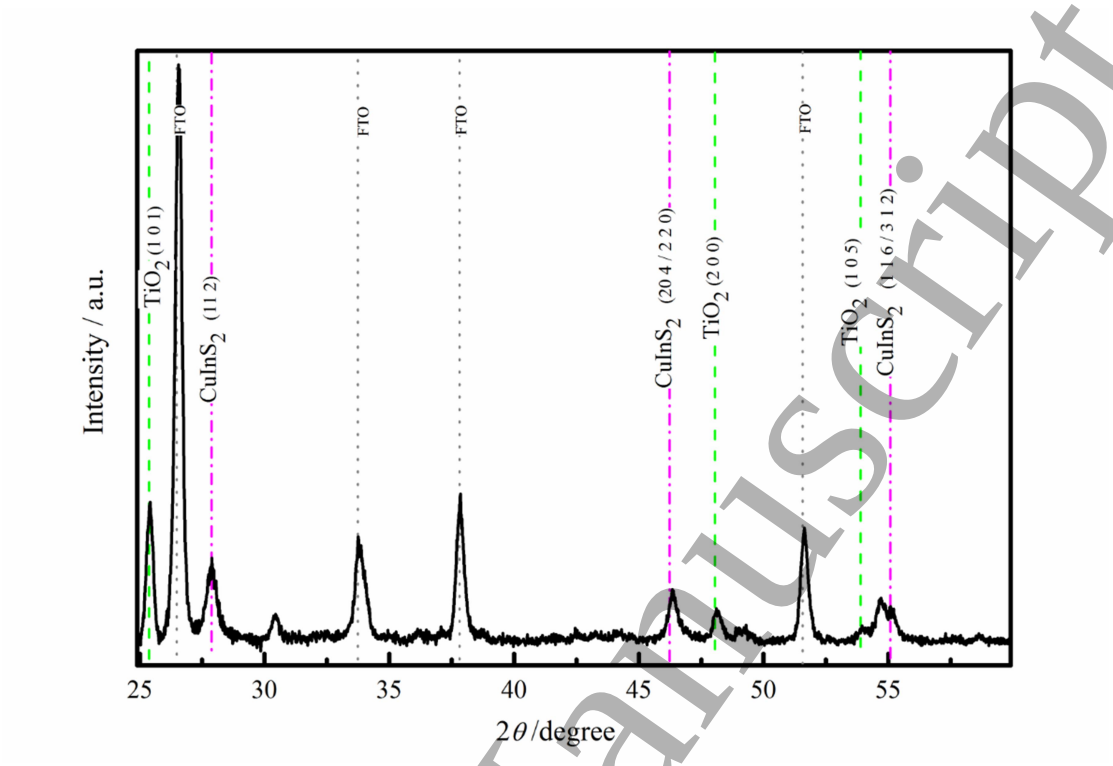

Figure 1: Grazing incidence X-ray diffractogram of CIS deposited onto FTO/TiO_2/In_2S_3 substrate by electrodeposition, after 60 min sulfurization (T = 500 º C) and 30 s etching in 0.5 mol L^{-1} KCN solution. Unlabeled peaks correspond to the K_β radiation from the X rays.

Raman spectroscopy is frequently used to provide complementary information to that from GXRD analysis. In this work quasi-resonant Raman scattering measurements were performed. The conditions can be achieved by selecting an excitation wavelength close enough to the band gap of the compound [32]. This leads to a strong increment in the intensity of the Raman modes. For the CIS layer, the spectrum measured with 785 nm excitation wavelength shows the resonant enhancement. This also includes the main vibrational mode from the Cu–Au (CA) ordered polytype.

Figure 2 shows the Raman spectrum measured in quasi-resonant conditions. This spectrum is characterized by the presence of four first order peaks in the 200–400 cm^{-1} spectral region, and three second order bands in the 550–750 cm^{-1} spectral region. The strong peaks at 290 and 307 cm^{-1} correspond to the A_1 mode of the chalcopyrite (CH) structure and the CA ordering, respectively [32], suggesting that both orders are present and mixed in this layer. Whereas in non-resonant excitation conditions the main mode at 340 cm^{-1} corresponds to the presence of $CuIn_5S_8$ spinel secondary phase, in resonant conditions the position of this contribution agrees with the $B_2^{(3)}(L)/E^{(6)}(L)$ $CuInS_2$ peak. The intensity of this band is related with the band gap and the amount of S in the alloy[32]. Table 1 lists the frequency of the different peaks from the experimental spectrum. A comparison of these data with those previously reported confirms the assignment of the bands. The vibration modes of In_2S_3 cannot be detected due to the small Raman cross sections and the small film thickness. β-In_2S_3 presents a main mode at 327 cm^{-1} corresponding to F_{2g} [29]. Thus, a weak signal could also be hidden by the four CIS peaks in the 200–400 cm^{-1} region.

Table 1: Frequency of the first and second order Raman modes with their corresponding $CuInS_2$ vibrational modes.

Raman shift / cm^{-1}	Assignment
258	$B_2^{(2)}(L) / E^{(4)}(L)$
290	A_1
307	$E^{(5)}(L)$
340	$B_2^{(3)}(L) / E^{(6)}(L)$
601	$[B_2^{(2)}(L) / E^{(4)}(L)] + [B_2^{(3)}(L) / E^{(6)}(L)]$
647	$E^{(5)}(L) + [B_2^{(3)}(L) / E^{(6)}(L)]$
681	$[B_2^{(3)}(L) / E^{(6)}(L)] + [B_2^{(3)}(L) / E^{(6)}(L)]$

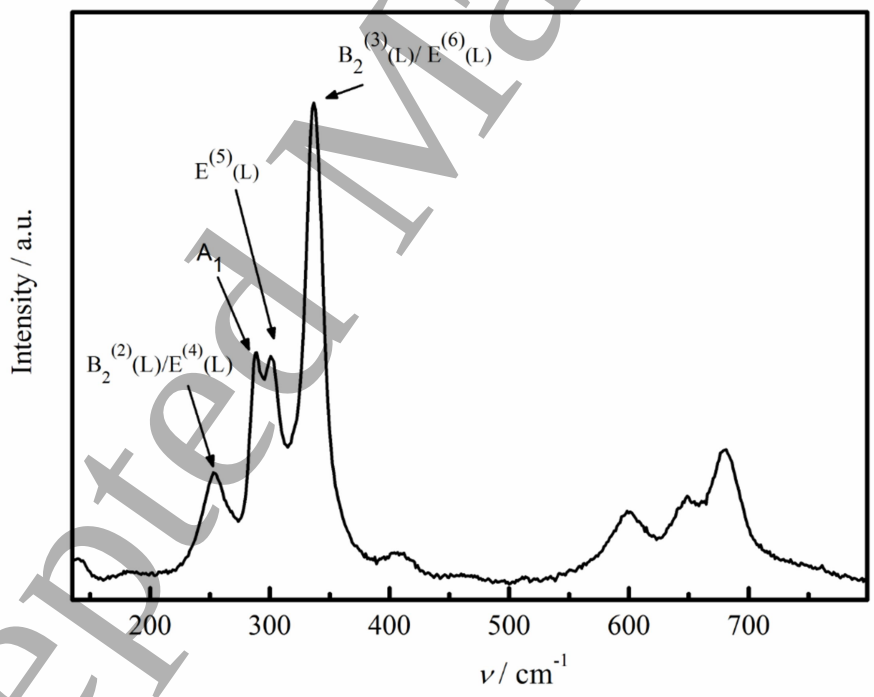

Figure 2: Raman spectrum measured with 785 nm excitation wavelength. The sample consists of CIS electrodeposited onto FTO/TiO_2/In_2S_3, after 60 min sulfurization (T = 500ºC) and 30 s etching in 0.5 mol L^{-1} KCN solution. See Table 1 for peak identification.

Figure 3 shows frontal and cross-section SEM images together with profilometry results. Figure 3a shows a SEM micrograph of TiO_2 deposited on FTO, while Figure 3b shows an image of the complete CIS solar cell (FTO/TiO_2/In_2S_3/CIS). The films present good coverage and the surface aspect is homogeneous. A cross-sectional view is presented in Figure 3c for the complete system. In this image, each layer can be clearly identified and their respective thicknesses can be evaluated: 360 nm for TiO_2 layer and 320 nm for the CIS absorbing layer.

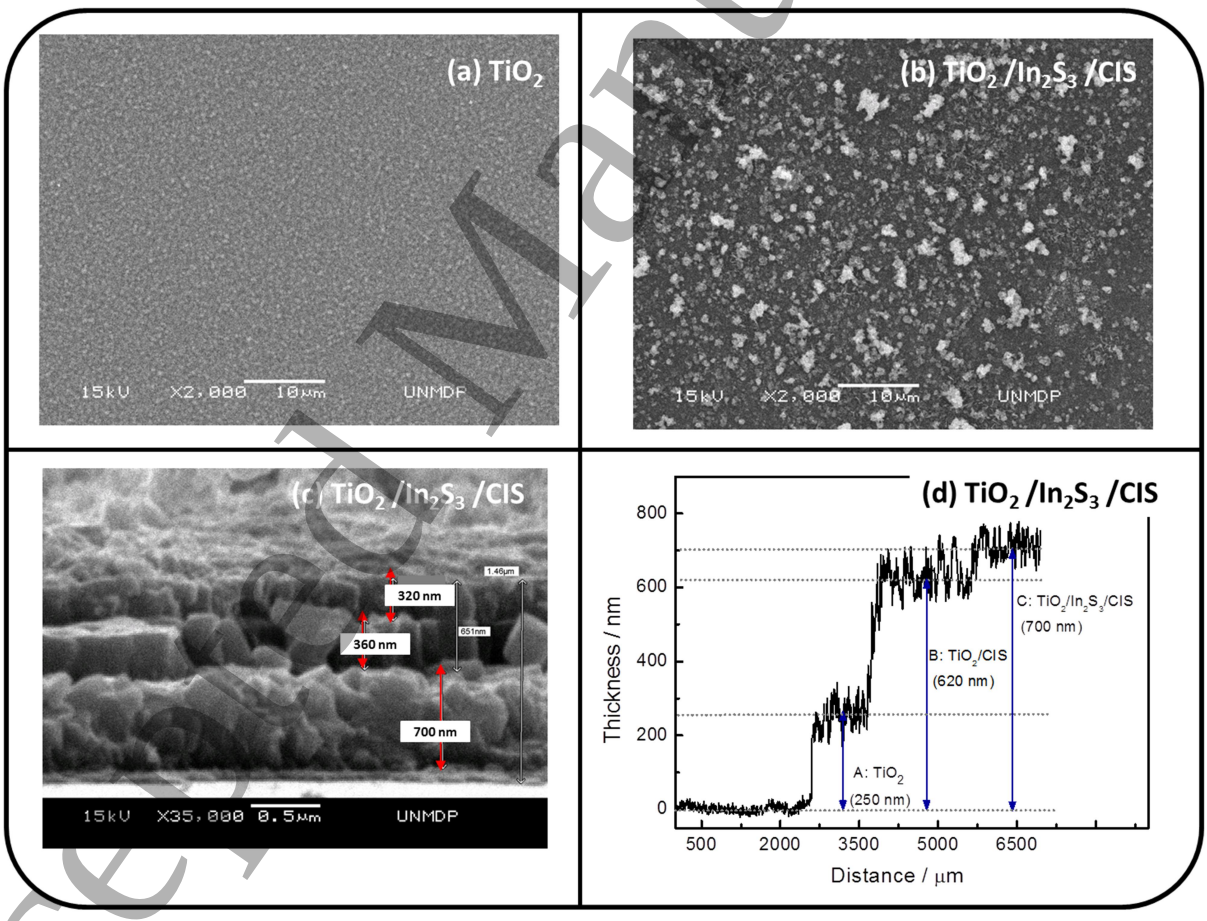

Figure 3: Surface morphology of (a) TiO_2 and (b) FTO/TiO_2/In_2S_3/CIS. (c) Cross-sectional view of FTO/TiO_2/In_2S_3/CIS cell. (d) Profilometric scan of the FTO/TiO_2/In_2S_3/CIS cell after annealing and etching.

These results are in agreement with the profilometric measurements (Figure 3d), where the average thicknesses are 250, 80 and 370 nm for TiO_2, In_2S_3 and CIS layers respectively. In order to use the profilometer, the sample was constructed so that the first part contained just TiO_2, the middle region CIS on top of TiO_2, and the final part comprised the complete combination (FTO/TiO_2/In_2S_3/CIS).

Figure 4 shows the optical transmittance (T) of the hetero-junction. To calculate the transmittance, a bare FTO/glass substrate was used as reference. The curve roughly shows the absorption edges corresponding to the TiO_2 and the $CuInS_2$ layer. The In_2S_3 layer is too thin to be appreciated. The bandgap energy (E_g) of each layer may be obtained from the corresponding absorption edge position, in good agreement with the values reported for the individual layers [3, 33].

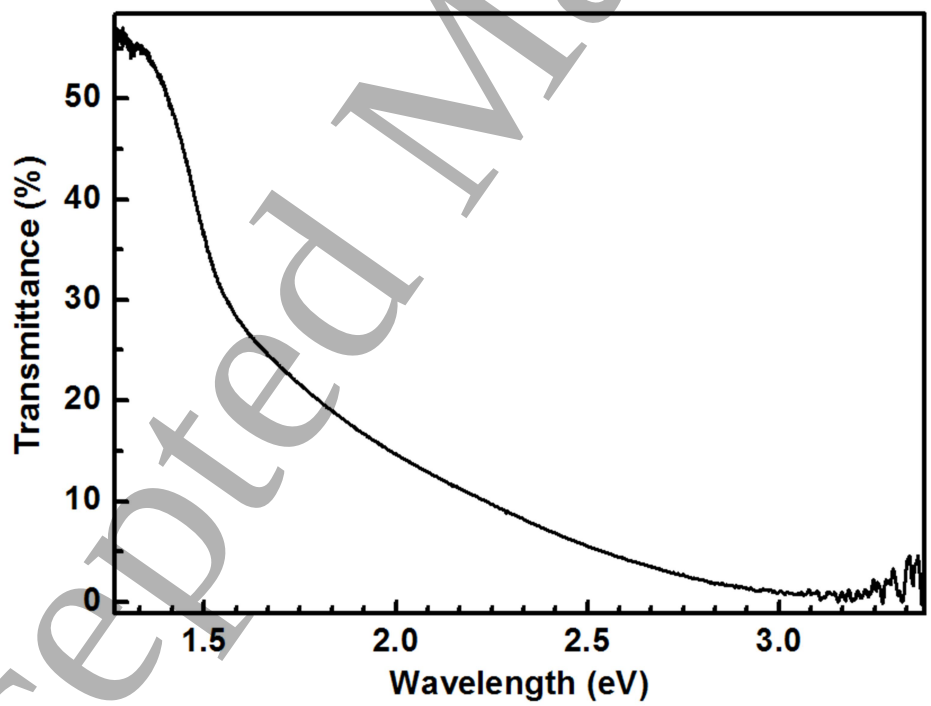

Figure 4. Transmittance spectrum of CIS deposited onto FTO/TiO_2/In_2S_3 substrate by electrodeposition, after 60 min sulfurization (T = 500 º C) and 30 s etching in 0.5 mol L^{-1} KCN solution.

The current density-voltage curve (*J*/V) characteristic of the FTO/TiO_2/In_2S_3/CIS/graphite cell was measured in the dark and under simulated solar irradiation in order to analyze the photovoltaic properties. Figure 5 shows the *J*-V response of the best device. In the dark, the device responded with typical diode behavior showing good rectification ratios. Under the effect of light, the best cell presented an open circuit voltage, Voc, of 0.583 V. The short-circuit current density *J*sc was 17.7 mA cm^{-2} and the fill factor FF 0.32. The energy conversion efficiency, calculated as $\eta = (Voc\ J_{SC}\ FF) / P_{in}$ is 3.3%. P_{in} is the input power, i.e. 100 mW cm^{-2}. Similar results were obtained for the five spots evaluated in the cell. Other cells presented similar results and the average efficiency was found to be between 1.5–2%. These results contrast with those obtained by O'Hayre et al., who found a 0.8% efficiency for their planar cell (no nanostructured layer) [11]. It is also worth mentioning that no significant difference between the curves with and without illumination was obtained in cells that did not include the In_2S_3 buffer layer (not shown), consistent with previous results [11]. The small fill factor may be associated to the high resistivity of some of the layers. It can also be due to high series resistance and/or low shunt resistance in the cells. In superstrate cells, the thickness of each of the layers is critical and it is known to affect the cell output characteristics and to ultimately govern the maximum efficiency. The impact of this parameter will be investigated in the near future. Also, the minority carrier lifetime in absorber layer may not be high enough. This is common in polycrystalline thin film PV absorber materials and can be improved by refining the grain size.

These promising results show that $CuInS_2$ thin films deposited by electrodeposition have an auspicious photovoltaic response, even better than that of similar cells [11, 20, 21,

[34]. The cell parameters and the deposition conditions still have significant room for optimization in the near future.

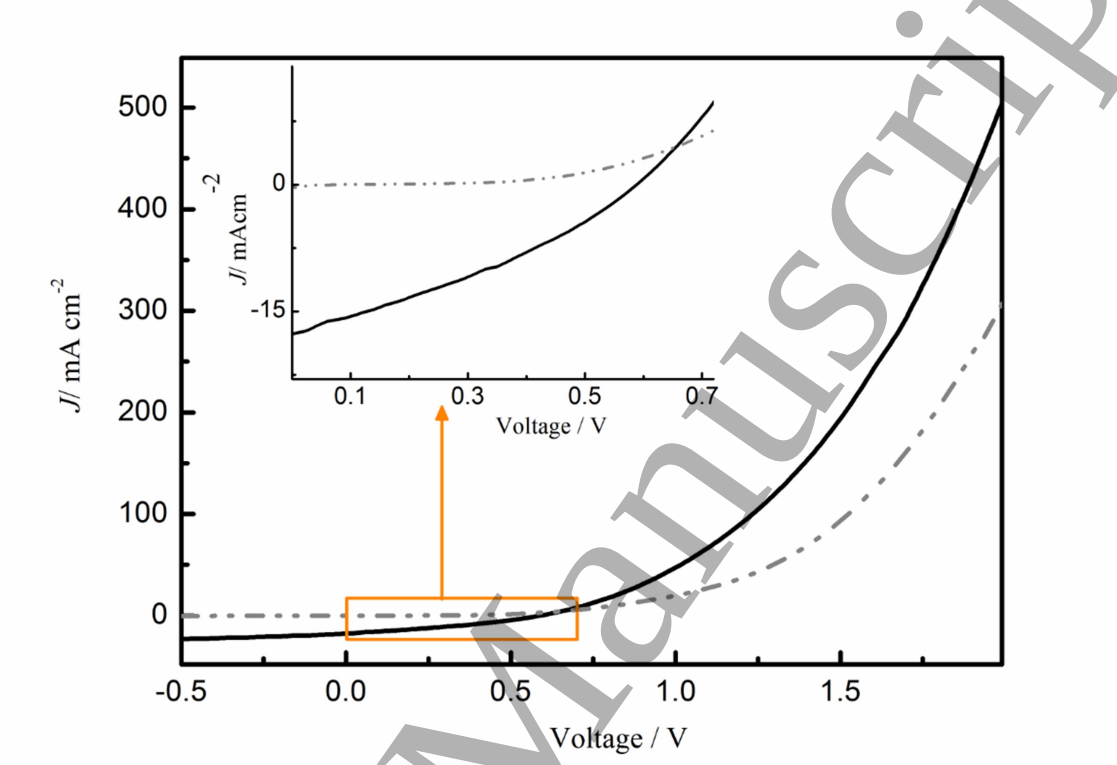

Figure 5: *J*–V curves in the dark (dash line) and under simulated solar irradiation (full line), corresponding to a device composed of FTO/TiO_2/In_2S_3/CIS/graphite) (1 sun).

4. CONCLUSIONS

An inexpensive methodology comprising chemical spray pyrolysis and electrodeposition has been used to prepare FTO/TiO_2/In_2S_3/CIS hetero-junctions in superstrate configuration. $CuInS_2$ thin films were grown from a single bath at pH 8 by one–step electrodeposition using FTO/TiO_2/In_2S_3 as substrate. According to the X-ray diffraction patterns and Raman spectra, the predominant phase in the absorbent layer corresponds to $CuInS_2$ chalcopyrite. The presence of In_2S_3 as buffer layer helped to

match the valence bands energy and to suppress the back flow of electrons. No photoresponse was detected in the absence of this buffer layer.

The open circuit potential and short circuit current density of the best solar cell resulted in a conversion energy efficiency of 3.3%. Current investigations aim at determining the films' resistance and to find the thickness values that can lead to an optimization the cell performance.

ACKNOWLEDGEMENTS

The authors acknowledge the financial support received from the Consejo Nacional de Investigaciones Científicas y Técnicas (CONICET), Agencia Nacional de Promoción Científica y Tecnológica (ANPCyT, PICT 2634), and Universidad Nacional de Mar del Plata (ING477/16). We are also grateful to Eng. Sheila Omar for her assistance with the profilometer.

REFERENCES

1. M. Theelen and F. Daume, *Solar Energy*, 2016, **133**, 586-627.
2. K. W. Cheng and W. H. Chiang, *Journal of Electroanalytical Chemistry*, 2011, **661**, 57-65.
3. Y. Di Iorio, M. Berruet, W. Schreiner and M. Vázquez, *Journal of Applied Electrochemistry*, 2014.
4. M. Nanu, L. Reijnen, B. Meester, A. Goossens and J. Schoonman, *Thin Solid Films*, 2003, **431-432**, 492-496.
5. J. Yuan, C. Shao, L. Zheng, M. Fan, H. Lu, C. Hao and D. Tao, *Vacuum*, 2014, **99**, 196-203.
6. M. Nanu, L. Reijnen, B. Meester, J. Schoonman and A. Goossens, *Chemical Vapor Deposition*, 2004, **10**, 45-49.
7. M. Nanu, J. Schoonman and A. Goossens, *Nano Letters*, 2005, **5**, 1716-1719.
8. N. Schneider, M. Bouttemy, P. Genevée, D. Lincot and F. Donsanti, *Nanotechnology*, 2015, **26**.
9. A. H. Cheshmekhavar, A. R. Mahjoub, H. Fakhri and M. Dehghani, *RSC Adv.*, 2015, **5**, 97381-97390.
10. M. Krunks, A. Katerski, T. Dedova, I. Oja Acik and A. Mere, *Solar Energy Materials and Solar Cells*, 2008, **92**, 1016-1019.
11. R. O'Hayre, M. Nanu, J. Schoonman and A. Goossens, *Nanotechnology*, 2007, **18**, 055702.
12. J. C. W. Ho, T. Zhang, K. K. Lee, S. K. Batabyal, A. I. Y. Tok and L. H. Wong, *ACS Applied Materials and Interfaces*, 2014, **6**, 6638-6643.
13. S. Ito and T. Ryo, *Advances in Materials Science and Engineering*, 2012, **2012**.

14. F. Thomazi, L. S. Roman, A. Ferreira Da Silva and C. Persson, *Physica Status Solidi (C) Current Topics in Solid State Physics*, 2009, **6**, 2740-2742.

15. L. Yang, Y. Ma, J. Liu and Y. Mai, *RSC Advances*, 2016, **6**, 92869-92873.

16. D. So, S. Pradhan and G. Konstantatos, *Nanoscale*, 2016, **8**, 16776-16785.

17. S. Higashimoto, T. Okada, T. Arase, M. Azuma, M. Yamamoto and M. Takahashi, *Electrochimica Acta*, 2016, **222**, 867-874.

18. Y. Liu, T. Chen, Z. Peng, L. Wu, K. Chen, P. Zhou, L. Wang and W. Chen, *Journal of Alloys and Compounds*, 2016, **658**, 76-84.

19. Z. Peng, Y. Liu, Y. Zhao, K. Chen, Y. Cheng and W. Chen, *Electrochimica Acta*, 2014, **135**, 276-283.

20. M. Dehghani, A. Behjat, F. Tajabadi and N. Taghavinia, *Journal of Physics D: Applied Physics*, 2015, **48**.

21. A. H. Cheshme khavar, A. Mahjoub, F. S. Samghabadi and N. Taghavinia, *Materials Chemistry and Physics*, 2017, **186**, 446-455.

22. A. H. Cheshme Khavar, A. R. Mahjoub, F. Tajabadi, M. Dehghani and N. Taghavinia, *European Journal of Inorganic Chemistry*, 2015, **2015**, 5793-5800.

23. D. C. Nguyen, T. Ryo and S. Ito, 2011.

24. M. Nanu, J. Schoonman and A. Goossens, *Advanced Functional Materials*, 2005, **15**, 95-100.

25. M. Valdés, M. Vázquez and A. Goossens, *Electrochimica Acta*, 2008, **54**, 524-529.

26. M. H. Valdés, M. Berruet, A. Goossens and M. Vázquez, *Surface and Coatings Technology*, 2010, **204**, 3995-4000.

27. M. Berruet, M. Valdés, S. Ceré and M. Vázquez, *Journal of Materials Science*, 2012, **47**, 2454-2460.

28. M. Valdés, M. A. Frontini, M. Vázquez and A. Goossens, *Applied Surface Science*, 2007, **254**, 303-307.

29. T. Sall, B. Marí Soucase, M. Mollar, B. Hartitti and M. Fahoume, *Journal of Physics and Chemistry of Solids*, 2015, **76**, 100-104.

30. M. Bär, J. Klaer, L. Weinhardt, R. G. Wilks, S. Krause, M. Blum, W. Yang, C. Heske and H.-W. Schock, *Advanced Energy Materials*, 2013, **3**, 777-781.

31. M. Valdés, A. Goossens and M. Vázquez, *Materials Chemistry and Physics*, 2011, **125**, 860-865.

32. J. Álvarez-García, J. Marcos-Ruzafa, A. Pérez-Rodríguez, A. Romano-Rodríguez, J. R. Morante and R. Scheer, *Thin Solid Films*, 2000, **361**, 208-212.

33. L. Castaeda, J. C. Alonso, A. Ortiz, E. Andrade, J. M. Saniger and J. G. Bauelos, *Materials Chemistry and Physics*, 2003, **77**, 938-944.

34. A. H. Cheshme Khavar, A. R. Mahjoub and H. Fakhri, *Journal of Inorganic and Organometallic Polymers and Materials*, 2016, **26**, 1075-1086.